Investigation of trapped thickness-twist waves induced by functionally graded piezoelectric material in an inhomogeneous plate

2013 Smart Mater. Struct. 22 095021

(http://iopscience.iop.org/0964-1726/22/9/095021)

Smart Mater. Struct. **22** (2013) 095021 (16pp) doi:10.1088/0964-1726/22/9/095021

Investigation of trapped thickness-twist waves induced by functionally graded piezoelectric material in an inhomogeneous plate

Peng Li[1], **Feng Jin**[1] **and Xiao-Shan Cao**[2]

[1] State Key Laboratory for Strength and Vibration of Mechanical Structures, School of Aerospace, Xi'an Jiaotong University, Xi'an 710049, People's Republic of China
[2] Department of Engineering Mechanics, School of Civil Engineering and Architecture, Xi'an University of Technology, Xi'an 710048, People's Republic of China

E-mail: jinfengzhao@263.net

Received 10 April 2013, in final form 28 June 2013
Published 29 August 2013
Online at stacks.iop.org/SMS/22/095021

Abstract
The effect of functional graded piezoelectric materials on the propagation of thickness-twist waves is investigated through equations of the linear theory of piezoelectricity. The elastic and piezoelectric coefficients, dielectric permittivity, and mass density are assumed to change in a linear form but with different graded parameters along the wave propagation direction. We employ the power-series technique to solve the governing differential equations with variable coefficients attributed to the different graded parameters and prove the correction and convergence of this method. As a special case, the functional graded middle layer resulting from piezoelectric damage and material bonding is investigated. Piezoelectric damaged material can facilitate energy trapping, which is impossible in perfect materials. The increase in the damaged length and the reduction in the piezoelectric coefficient decrease the resonance frequency but increase the number of modes. Higher modes of thickness-twist waves appear periodically along the damaged length. Moreover, the displacement of the center of the damaged portion is neither symmetric nor anti-symmetric, unlike the non-graded plate. The conclusions are theoretically and practically significant for wave devices.

(Some figures may appear in colour only in the online journal)

1. Introduction

Thickness-twist vibration modes are anti-plane or shear horizontal (SH) modes in plates that are often used as the operating modes for resonators, filters, and acoustic wave sensors made from quartz and polarized ceramics [1, 2]. The frequencies of such waves are mainly determined by the plate thickness, which is the smallest dimension of the plate [3]. When a sixfold axis of a 6 mm crystal is parallel to the major surface of a plate, thickness-twist waves can propagate in both a homogeneous piezoelectric plate [4] and an inhomogeneous piezoelectric plate [5, 6].

In the 1980s, a new kind of material called functionally graded material (FGM) was proposed to solve the problems that arise in the thermal-protection systems of aerospace structures. Since then, the FGM structure has increasingly attracted the attention of scientists and engineers. FGM continues to be used in thermal-protection systems [7] as well as in electronics and in most advanced integrated systems for vibration control and health monitoring [8]. Since 1991, functionally graded piezoelectric material (FGPM) has been manufactured [9] and applied to surface acoustic wave devices for efficiency and sensitivity improvement. For example, functional graded piezoelectric transducers have been found

to generate an ultrasonic wave with a broader frequency spectrum than conventional transducers [10].

However, during material manufacture and application, the possible defects of impurity, cavities, and micro-cracks as well as the corrosive environment and fatigue under periodic mechanical or thermal loading result in the subsurface damage of the piezoelectric materials [11]. This process makes the material coefficients inhomogeneous, thus transforming the original material into an FGPM.

The effect of FGPM on wave propagation, including the Love, Bleustein–Gulyaev, Rayleigh, and Lamb waves, has been extensively investigated. Collet *et al* considered Bleustein–Gulyaev waves in a functionally graded piezoelectric half-space [12]. Du *et al* discussed the features of Love waves in a layered functionally graded piezoelectric structure [13]. Similarly, the propagation of this kind of SH waves near the interface between two functionally graded piezoelectric half-spaces under electroded and unelectroded conditions has been investigated [14]. The assumption that all material coefficients change in the same exponential function variation is usually adopted for analytical simplification [12–16]. However, this kind of variation pattern is almost impossible in actuality. For other material patterns, the main methods include the inhomogeneous layer element method [17], multilayered approximation [18], Wentzel–Kramers–Brillouin asymptotic approximation technique [19–21], Legendre polynomial approach [22, 23], equivalent network representation [24], homotopy analysis method [25], etc. Other matrix methods such as the state-vector formulation [26], stiffness matrix method [27], and reverberation-ray matrix method [28] can also be used to calculate waves in FGPM, based on the multilayered approximation. The power-series technique has recently been used for the asymptotic analytical derivation of the governing equation of a transverse surface wave [29].

Among all aforementioned FGPMs, the material coefficients shift along the thickness direction [12–29]. FGPMs in which the material changes along the length or width direction has not been widely investigated despite its possible use in device applications. For example, the stress concentration at actuator edges can be significantly reduced or essentially removed in FGPM actuators by changing their material characteristics in the length direction [30].

In this paper, we discuss the effect of FGPM, which is located in the middle region of an inhomogeneous plate, on thickness-twist wave propagation. The material coefficients change linearly but with different parameters in the length direction. This linear pattern can be used to simulate the effect of FGPM induced by internal temperature variations [24]. The power-series technique is adopted to solve this problem. Moreover, correction and convergence are proven theoretically. As a special case, the FGPM attributed to piezoelectric damage as well as an FGPM buffer layer is discussed. Considering that the material tensors of crystals with 6 mm symmetry possess the same structures as polarized ceramics, our analysis is also valid for 6 mm piezoelectric crystals such as ZnO and AlN.

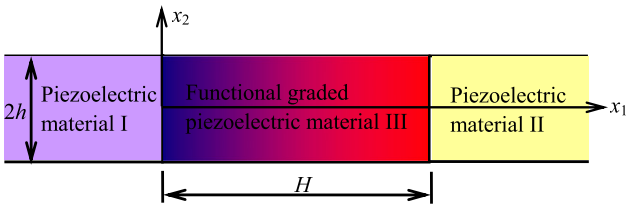

Figure 1. Inhomogeneous transversely piezoelectric plate with a functionally graded piezoelectric layer in the central portion.

2. Governing equations and propagating wave solutions

The propagation of thickness-twist waves in an inhomogeneous piezoelectric plate of 6 mm crystals or polarized ceramics with a depth of $2h$ is considered, as shown in figure 1. The plate comprises a FGPM in the region $0 < x_1 < H$ and two different transversely piezoelectric materials in the outer portions $x_1 < 0$ and $x_1 > H$. All piezoelectric materials are poled in the x_3 direction determined by the right-hand rule from the x_1 and x_2 axes. The material coefficients of the point change along the wave propagation direction, i.e., the x_1 direction, not the depth direction, which differs from previous works [12–29].

The thickness-twist mode can be represented by the displacement component $\boldsymbol{u}$ and electrical potential function φ as follows [1, 5, 6]:

$$\begin{gathered} u_1 = u_2 = 0, \qquad u_3 = u(x_1, x_2, t), \\ \varphi = \varphi(x_1, x_2, t) \end{gathered} \tag{1}$$

where $\boldsymbol{u}$ is the displacement vector and φ is the electric potential function. The linear piezoelectric constitutive equations can be expressed as [31]

$$\begin{aligned} \sigma_{ij} &= c_{ijkl} u_{k,l} + e_{lij} \varphi_{,l} \\ D_i &= e_{ikl} u_{k,l} - \varepsilon_{il} \varphi_{,l} \end{aligned} \tag{2}$$

where σ_{ij} and D_i are the stress tensors and the electrical displacement vector, respectively; and c_{ijkl}, e_{lij}, and ε_{il} are the elastic and piezoelectric coefficients, and dielectric permittivity, respectively. An index after a comma denotes a partial differentiation with respect to the coordinate.

2.1. Solutions for the left region $x_1 < 0$

In this work, we use the '$*$' and '$'$' symbols to distinguish the different parameters associated with the outer portions $x_1 < 0$ and $x_1 > H$, respectively. In the left region $x_1 < 0$, the governing equations for u^* and φ^* are [13, 14]

$$\begin{aligned} c_{44}^* \nabla^2 u^* + e_{15}^* \nabla^2 \varphi^* &= \rho^* \ddot{u}^* \\ e_{15}^* \nabla^2 u^* - \varepsilon_{11}^* \nabla^2 \varphi^* &= 0 \end{aligned} \tag{3}$$

where $\nabla^2 = \partial^2/\partial x_1^2 + \partial^2/\partial x_2^2$ is the Laplace operator, and the dot refers to time differentiation. The solutions for the trapped thickness-twist waves in the x_1 direction can be expressed

as [5]

$$\begin{aligned} u^* &= A_1^* \mathrm{e}^{\xi_1^* x_1} \cos(\xi_2 x_2) \exp(-\mathrm{i}\omega t) \\ \varphi^* &= \left(\frac{e_{15}^*}{\varepsilon_{11}^*} A_1^* \mathrm{e}^{\xi_1^* x_1} + B_1^* \mathrm{e}^{\xi_2 x_1} \right) \cos(\xi_2 x_2) \exp(-\mathrm{i}\omega t) \end{aligned} \tag{4}$$

where A_1^* and B_1^* are undetermined constants; ξ_1^* and ξ_2 are wavenumbers in the x_1 and x_2 directions, respectively; $\xi_2 = \frac{m\pi}{2h}$ $(m = 0, 2, 4, \ldots)$; ω is the wave frequency; and $\mathrm{i}^2 = -1$. Similarly, the corresponding anti-symmetric modes in the x_2 direction can be obtained using $\sin(\xi_2 x_2)$ and $\xi_2 = \frac{m\pi}{2h}$ $(m = 1, 3, 5, \ldots)$. Generally speaking, $m = 0$ is called the face-shear wave, and $m > 0$ is related to the thickness-twist wave [5, 6]. In particular, the face-shear mode, i.e., $m = 0$, will not be considered in the following discussion, and only the symmetric thickness-twist modes in the x_2 direction, i.e., where m is even number, is discussed in present contribution for simplification. Inserting equation (4) into (3) yields

$$\xi_1^* = \sqrt{\xi_2^2 - \frac{\rho^* \omega^2}{\bar{c}_{44}^*}} = \frac{1}{c_{\mathrm{sh}}^*} \sqrt{\omega_{\mathrm{m}}^{*2} - \omega^2} \tag{5}$$

where $c_{\mathrm{sh}}^* = \sqrt{\bar{c}_{44}^*/\rho^*}$ and $\omega_{\mathrm{m}}^* = \left(\frac{m\pi}{2h}\right) c_{\mathrm{sh}}^*$ are respectively the bulk shear wave velocity and the corresponding cut-off frequency of the thickness-twist waves for the piezoelectric material occupying $x_1 < 0$. Substituting equation (4) into (2), the stress component T_{31}^*, and electrical displacement D_1^* can be obtained as

$$\begin{aligned} T_{31}^* &= (\bar{c}_{44}^* \xi_1^* A_1^* \mathrm{e}^{\xi_1^* x_1} + e_{15}^* \xi_2 B_1^* \mathrm{e}^{\xi_2 x_1}) \\ &\quad \times \cos(\xi_2 x_2) \exp(-\mathrm{i}\omega t) \\ D_1^* &= -\varepsilon_{11}^* \xi_2 B_1^* \mathrm{e}^{\xi_2 x_1} \cos(\xi_2 x_2) \exp(-\mathrm{i}\omega t). \end{aligned} \tag{6}$$

2.2. Solutions for the right region $x_1 > H$

Similarly to the left portion, the governing equations for u' and φ' of the right portion $x_1 > H$ are [20]

$$\begin{aligned} c_{44}' \nabla^2 u' + e_{15}' \nabla^2 \varphi' &= \rho' \ddot{u}' \\ e_{15}' \nabla^2 u' - \varepsilon_{11}' \nabla^2 \varphi' &= 0. \end{aligned} \tag{7}$$

The symmetric modes in the x_2 direction for the trapped thickness-twist waves propagating in the x_1 direction can also be expressed as [6]

$$\begin{aligned} u' &= A_1' \mathrm{e}^{-\xi_1'(x_1 - H)} \cos(\xi_2 x_2) \exp(-\mathrm{i}\omega t) \\ \varphi' &= \left[\frac{e_{15}'}{\varepsilon_{11}'} A_1' \mathrm{e}^{-\xi_1'(x_1 - H)} + B_1' \mathrm{e}^{-\xi_2(x_1 - H)} \right] \\ &\quad \times \cos(\xi_2 x_2) \exp(-\mathrm{i}\omega t) \end{aligned} \tag{8}$$

where A_1' and B_1' are undetermined constants, and ξ_1' is wavenumber in the x_1 direction. Inserting equation (8) into (7) yields

$$\xi_1' = \sqrt{\xi_2^2 - \frac{\rho' \omega^2}{\bar{c}_{44}'}} = \frac{1}{c_{\mathrm{sh}}'} \sqrt{\omega_{\mathrm{m}}'^2 - \omega^2} \tag{9}$$

where $c_{\mathrm{sh}}' = \sqrt{\bar{c}_{44}'/\rho'}$ and $\omega_{\mathrm{m}}' = \left(\frac{m\pi}{2h}\right) c_{\mathrm{sh}}'$ are respectively the bulk shear wave velocity and the corresponding cut-off frequency for the right region $x_1 > H$. Based on these solutions, the stress and electrical displacement components are

$$\begin{aligned} T_{31}' &= [-\bar{c}_{44}' \xi_1' A_1' \mathrm{e}^{-\xi_1'(x_1 - H)} - e_{15}' \xi_2 B_1' \mathrm{e}^{-\xi_2(x_1 - H)}] \\ &\quad \times \cos(\xi_2 x_2) \exp(-\mathrm{i}\omega t) \\ D_1' &= \varepsilon_{11}' \xi_2 B_1' \mathrm{e}^{-\xi_2(x_1 - H)} \cos(\xi_2 x_2) \exp(-\mathrm{i}\omega t). \end{aligned} \tag{10}$$

2.3. Solutions for the FGPM region $0 < x_1 < H$

In the FGPM layer, regardless of the variation that facilitates material parameter changes along the x_1 direction, such changes can be theoretically expressed into the power function using Taylor's series expansion

$$\begin{aligned} c_{44} &= \sum_{n=0}^{\infty} c_{44}^{(n)} \left(\frac{x_1}{H}\right)^n, & e_{15} &= \sum_{n=0}^{\infty} e_{15}^{(n)} \left(\frac{x_1}{H}\right)^n, \\ \varepsilon_{11} &= \sum_{n=0}^{\infty} \varepsilon_{11}^{(n)} \left(\frac{x_1}{H}\right)^n, & \rho &= \sum_{n=0}^{\infty} \rho^{(n)} \left(\frac{x_1}{H}\right)^n. \end{aligned} \tag{11}$$

In this work, only the two terms are retained for all the material coefficients, i.e., the elastic, piezoelectric, and dielectric coefficients as well as the mass density of the FGPM are all assumed to change linearly in the x_1 direction:

$$\begin{aligned} c_{44} &= c_{44}^0 \left(1 - \alpha \frac{x_1}{H}\right), & e_{15} &= e_{15}^0 \left(1 - \beta \frac{x_1}{H}\right), \\ \varepsilon_{11} &= \varepsilon_{11}^0 \left(1 - \gamma \frac{x_1}{H}\right), & \rho &= \rho^0 \left(1 - \eta \frac{x_1}{H}\right) \end{aligned} \tag{12}$$

where the coefficients α, β, γ, and η indicate the profile of the corresponding material gradient along the x_1-axis, and the quantities with superscript '0' are the values of these parameters at $x_1 = 0$. This linear pattern can be used to calculate the effect of FGPM induced by internal temperature variations [24]. The investigation and understanding of the effect of the graded factor on the characteristics of thickness-twist wave propagation is of great importance.

The displacement u and electrical potential φ in the FGPM middle layer $0 < x_1 < H$ can be expressed as

$$\begin{aligned} u &= U(x_1) \cos(\xi_2 x_2) \exp(-\mathrm{i}\omega t) \\ \varphi &= \Phi(x_1) \cos(\xi_2 x_2) \exp(-\mathrm{i}\omega t). \end{aligned} \tag{13}$$

Thus, the governing equations are [21, 22]

$$\begin{aligned} &c_{44} \left(\frac{\mathrm{d}^2 U}{\mathrm{d}x_1^2} - \xi_2^2 U \right) + e_{15} \left(\frac{\mathrm{d}^2 \Phi}{\mathrm{d}x_1^2} - \xi_2^2 \Phi \right) \\ &\quad + \frac{\mathrm{d}c_{44}}{\mathrm{d}x_1} \frac{\mathrm{d}U}{\mathrm{d}x_1} + \frac{\mathrm{d}e_{15}}{\mathrm{d}x_1} \frac{\mathrm{d}\Phi}{\mathrm{d}x_1} = \rho \ddot{U} \\ &e_{15} \left(\frac{\mathrm{d}^2 U}{\mathrm{d}x_1^2} - \xi_2^2 U \right) - \varepsilon_{11} \left(\frac{\mathrm{d}^2 \Phi}{\mathrm{d}x_1^2} - \xi_2^2 \Phi \right) \\ &\quad + \frac{\mathrm{d}e_{15}}{\mathrm{d}x_1} \frac{\mathrm{d}U}{\mathrm{d}x_1} - \frac{\mathrm{d}\varepsilon_{11}}{\mathrm{d}x_1} \frac{\mathrm{d}\Phi}{\mathrm{d}x_1} = 0. \end{aligned} \tag{14}$$

Equation (14) contains two second-order partial differential equations with variable coefficients with respect to U and Φ. Solving the equations directly is a difficult task. In this work, an asymptotic numerical solution can be obtained

from the power function expansion technique along the x_1 direction [11, 29, 32]

$$U(x_1) = \sum_{n=0}^{\infty} a_n \left(\frac{x_1}{H}\right)^n, \qquad \Phi(x_1) = \sum_{n=0}^{\infty} b_n \left(\frac{x_1}{H}\right)^n. \quad (15)$$

Substituting equations (12) and (15) into (14) yields

$$\begin{aligned} & c_{44}^0 \left(1-\alpha\frac{x_1}{H}\right) \sum_{n=0}^{\infty} [(n+2)(n+1)a_{n+2} - (\xi_2 H)^2 a_n] \left(\frac{x_1}{H}\right)^n \\ & + e_{15}^0 \left(1-\beta\frac{x_1}{H}\right) \sum_{n=0}^{\infty} [(n+2)(n+1)b_{n+2} \\ & - (\xi_2 H)^2 b_n] \left(\frac{x_1}{H}\right)^n - \sum_{n=0}^{\infty} (n+1)(c_{44}^0 \alpha a_{n+1} \\ & + e_{15}^0 \beta b_{n+1}) \left(\frac{x_1}{H}\right)^n + \rho^0 \left(1-\eta\frac{x_1}{H}\right) \omega^2 H^2 \\ & \times \sum_{n=0}^{\infty} a_n \left(\frac{x_1}{H}\right)^n = 0, \end{aligned} \quad (16a)$$

$$\begin{aligned} & e_{15}^0 \left(1-\beta\frac{x_1}{H}\right) \sum_{n=0}^{\infty} [(n+2)(n+1)a_{n+2} \\ & - (\xi_2 H)^2 a_n] \left(\frac{x_1}{H}\right)^n - \varepsilon_{11}^0 \left(1-\gamma\frac{x_1}{H}\right) \\ & \times \sum_{n=0}^{\infty} [(n+2)(n+1)b_{n+2} - (\xi_2 H)^2 b_n] \left(\frac{x_1}{H}\right)^n \\ & - \sum_{n=0}^{\infty} (n+1)(e_{15}^0 \beta a_{n+1} - \varepsilon_{11}^0 \gamma b_{n+1}) \left(\frac{x_1}{H}\right)^n = 0. \end{aligned} \quad (16b)$$

By equating the coefficients of $\left(\frac{x_1}{H}\right)^n$ in equation (16) to zero, we can obtain two cases for the corresponding recursive relationships of a_n and b_n:

$$\begin{aligned} a_2 &= \frac{1}{2}\left[\left(\frac{c_{44}^0}{\bar{c}_{44}^0}\alpha + k_e^2\beta\right) a_1 + \frac{e_{15}^0}{\bar{c}_{44}^0}(\beta-\gamma) b_1 \right. \\ &\quad \left. + \left(1 - \frac{\omega^2}{\omega_m^2}\right)(\xi_2 H)^2 a_0\right], \\ b_2 &= \frac{1}{2}\left[\frac{c_{44}^0}{\bar{c}_{44}^0}\frac{e_{15}^0}{\varepsilon_{11}^0}(\alpha-\beta) a_1 + \left(\frac{c_{44}^0}{\bar{c}_{44}^0}\gamma + k_e^2\beta\right) b_1 \right. \\ &\quad \left. - \frac{e_{15}^0}{\varepsilon_{11}^0}\frac{\omega^2}{\omega_m^2}(\xi_2 H)^2 a_0 + (\xi_2 H)^2 b_0\right] \end{aligned} \quad (17a)$$

$$\begin{aligned} a_{n+3} &= \frac{1}{(n+3)(n+2)}\left[(n+2)^2\left(\frac{c_{44}^0}{\bar{c}_{44}^0}\alpha + k_e^2\beta\right) a_{n+2} \right. \\ &\quad + (n+2)^2 \frac{e_{15}^0}{\bar{c}_{44}^0}(\beta-\gamma) b_{n+2} + \left(1 - \frac{\omega^2}{\omega_m^2}\right)(\xi_2 H)^2 a_{n+1} \\ &\quad - \left(\frac{c_{44}^0}{\bar{c}_{44}^0}\alpha + k_e^2\beta - \eta\frac{\omega^2}{\omega_m^2}\right)(\xi_2 H)^2 a_n \\ &\quad \left. - \frac{e_{15}^0}{\bar{c}_{44}^0}(\beta-\gamma)(\xi_2 H)^2 b_n\right], \end{aligned}$$

$$\begin{aligned} b_{n+3} &= \frac{1}{(n+3)(n+2)}\left\{(n+2)^2 \frac{c_{44}^0}{\bar{c}_{44}^0}\frac{e_{15}^0}{\varepsilon_{11}^0}(\alpha-\beta) a_{n+2} \right. \\ &\quad + (n+2)^2\left(\frac{c_{44}^0}{\bar{c}_{44}^0}\gamma + k_e^2\beta\right) b_{n+2} \\ &\quad - \frac{e_{15}^0}{\varepsilon_{11}^0}\frac{\omega^2}{\omega_m^2}(\xi_2 H)^2 a_{n+1} + (\xi_2 H)^2 b_{n+1} \\ &\quad - \frac{e_{15}^0}{\varepsilon_{11}^0}\left[\frac{c_{44}^0}{\bar{c}_{44}^0}(\alpha-\beta) - \eta\frac{\omega^2}{\omega_m^2}\right](\xi_2 H)^2 a_n \\ &\quad \left. - \left(\frac{c_{44}^0}{\bar{c}_{44}^0}\gamma + k_e^2\beta\right)(\xi_2 H)^2 b_n\right\} \end{aligned} \quad (17b)$$

where $\omega_m = \left(\frac{m\pi}{2h}\right) c_{sh}^0$, $k_e^2 = \frac{e_{15}^{0\,2}}{\varepsilon_{11}^0 \bar{c}_{44}^0}$, $\bar{c}_{44}^0 = c_{44}^0 + \frac{e_{15}^{0\,2}}{\varepsilon_{11}^0}$, and $c_{sh}^0 = \sqrt{\bar{c}_{44}^0/\rho^0}$ are the respective cut-off frequency, electromechanical coupling constant, effective piezoelectric stiffness, and bulk shear wave velocity when the middle layer is homogeneous. $n \geq 0$. a_0, a_1, b_0, b_1 are undetermined coefficients. Once these parameters are calculated, a_n and b_n $(n > 1)$ can be obtained using equation (17). Based on the given solutions, the solutions for the FGPM middle layer are

$$\begin{aligned} u &= \sum_{n=0}^{\infty} a_n \left(\frac{x_1}{H}\right)^n \cos(\xi_2 x_2) \exp(-\mathrm{i}\omega t) \\ \varphi &= \sum_{n=0}^{\infty} b_n \left(\frac{x_1}{H}\right)^n \cos(\xi_2 x_2) \exp(-\mathrm{i}\omega t). \end{aligned} \quad (18)$$

Similarly, the stress and electrical displace components are

$$\begin{aligned} T_{31} &= \frac{1}{H}\sum_{n=0}^{\infty}(n+1)\left[c_{44}^0\left(1-\alpha\frac{x_1}{H}\right) a_{n+1} \right. \\ &\quad \left. + e_{15}^0\left(1-\beta\frac{x_1}{H}\right) b_{n+1}\right]\left(\frac{x_1}{H}\right)^n \cos(\xi_2 x_2)\exp(-\mathrm{i}\omega t) \\ D_1 &= \frac{1}{H}\sum_{n=0}^{\infty}(n+1)\left[e_{15}^0\left(1-\beta\frac{x_1}{H}\right) a_{n+1} \right. \\ &\quad \left. - \varepsilon_{11}^0\left(1-\gamma\frac{x_1}{H}\right) b_{n+1}\right]\left(\frac{x_1}{H}\right)^n \cos(\xi_2 x_2)\exp(-\mathrm{i}\omega t). \end{aligned} \quad (19)$$

2.4. Boundary conditions and the frequency equation

- For unelectroded and traction-free surfaces at $x_2 = \pm h$ [5, 6]

$$T_{32}^* = T_{32} = T_{32}' = 0, \qquad D_2^* = D_2 = D_2' = 0. \quad (20)$$

- The continuity conditions at $x_1 = 0$ and H are

$$\begin{aligned} T_{31}^*(0, x_2) &= T_{31}(0, x_2), & D_1^*(0, x_2) &= D_1(0, x_2), \\ u^*(0, x_2) &= u(0, x_2), & \varphi^*(0, x_2) &= \varphi(0, x_2) \\ T_{31}(H, x_2) &= T_{31}'(H, x_2), \\ D_1(H, x_2) &= D_1'(H, x_2), \\ u(H, x_2) &= u'(H, x_2), & \varphi(H, x_2) &= \varphi'(H, x_2). \end{aligned} \quad (21)$$

Table 1. Frequencies (10^6 s^{-1}) of the plate for the homogeneous middle layer ($\alpha = \beta = \gamma = \eta = 0$) by using the power function expansion method.

n	15	20	25	30	35
$H = 4$ mm	3.513 887 98	3.513 167 48	3.513 171 98	3.513 171 98	3.513 171 98
n	30	35	40	45	50
$H = 8$ mm	3.419 222 48 3.590 959 48	3.420 125 48 3.587 845 48	3.420 116 98 3.587 873 98	3.420 116 98 3.587 873 98	3.420 116 98 3.587 873 98
n	50	55	60	65	70
$H = 12$ mm	3.390 914 98 3.484 472 98 3.626 357 98	3.390 935 48 3.484 395 48 3.626 508 98	3.390 935 48 3.484 395 98 3.626 507 98	3.390 935 48 3.484 395 98 3.626 507 98	3.390 935 48 3.484 395 98 3.626 507 98
n	65	70	75	80	85
$H = 16$ mm	3.378 487 98 3.436 604 48 3.530 517 98 3.649 370 48	3.378 424 48 3.436 849 48 3.529 992 48 3.650 192 98	3.378 424 98 3.436 847 98 3.529 996 48 3.650 186 48	3.378 424 98 3.436 847 98 3.529 996 48 3.650 186 98	3.378 424 98 3.436 847 98 3.529 996 48 3.650 186 98

Table 2. Frequencies (10^6 s^{-1}) of the plate for some special cases by using the power function expansion method ($H = 4$ mm).

n	15	20	25	30	35
$\alpha = 0.5$ $\beta = \gamma = \eta = 0$	3.211 213 51 3.659 678 01	3.211 240 01 3.664 782 51	3.211 238 51 3.664 741 51	3.211 238 51 3.664 741 51	3.211 238 51 3.664 741 51
$\beta = 0.5$ $\alpha = \gamma = \eta = 0$	3.299 378 82 3.695 769 32	3.298 076 32 3.694 405 32	3.298 081 32 3.694 366 82	3.298 081 32 3.694 366 82	3.298 081 32 3.694 366 82
$\gamma = 0.5$ $\alpha = \beta = \eta = 0$	3.633 582 48	3.633 785 98	3.633 784 98	3.633 784 98	3.633 784 98
$\eta = 0.5$ $\alpha = \beta = \gamma = 0$	3.720 828 98	3.721 538 48	3.721 535 48	3.721 535 48	3.721 535 48
$\alpha = 0.25$ $\beta = \gamma = \eta = 0$	3.379 698 79	3.379 058 29	3.379 062 29	3.379 062 29	3.379 062 29
$\alpha = \beta = 0.25$ $\gamma = \eta = 0$	3.245 416 64 3.672 685 14	3.244 902 64 3.675 575 14	3.244 906 14 3.675 581 14	3.244 906 14 3.675 580 64	3.244 906 14 3.675 580 64
$\alpha = \beta = \gamma = 0.25$ $\eta = 0$	3.313 585 54 3.709 990 54	3.313 234 04 3.710 465 04	3.313 236 54 3.710 465 54	3.313 236 54 3.710 465 54	3.313 236 54 3.710 465 54
$\alpha = \beta = \gamma = \eta = 0.25$	3.523 126 48	3.522 632 98	3.522 635 98	3.522 635 98	3.522 635 98

- The attenuation conditions at $x_1 \to \pm\infty$ are

$$\begin{aligned} u^*(-\infty, x_2) &\to 0, & \varphi^*(-\infty, x_2) &\to 0 \\ u'(\infty, x_2) &\to 0, & \varphi'(\infty, x_2) &\to 0. \end{aligned} \tag{22}$$

Equations (4), (8), and (18) satisfy the unelectroded and traction-free surface and attenuation conditions, i.e., equations (20) and (22). Substituting the displacement and electrical potential expressions equations (4), (8), and (18), as well as their corresponding stress and electric displacement components equations (6), (10), and (19), into the continuity condition equation (21) yields eight linear homogeneous algebraic equations for coefficients A_1^*, B_1^*, a_0, a_1, b_0, b_1, A_1', and B_1':

$$\begin{aligned} &\bar{c}_{44}^*(\xi_1^* H)A_1^* + e_{15}^*(\xi_2 H)B_1^* = c_{44}^0 a_1 + e_{15}^0 b_1, \\ &-\varepsilon_{11}^*(\xi_2 H)B_1^* = e_{15}^0 a_1 - \varepsilon_{11}^0 b_1, \\ &A_1^* = a_0, \qquad \frac{e_{15}^*}{\varepsilon_{11}^*}A_1^* + B_1^* = b_0, \\ &\sum_{n=0}^{\infty}(n+1)[c_{44}^0(1-\alpha)a_{n+1} + e_{15}^0(1-\beta)b_{n+1}] \\ &\quad = -\bar{c}_{44}'(\xi_1' H)A_1' - e_{15}'(\xi_2 H)B_1', \\ &\sum_{n=0}^{\infty}(n+1)[e_{15}^0(1-\beta)a_{n+1} - \varepsilon_{11}^0(1-\gamma)b_{n+1}] \\ &\quad = \varepsilon_{11}'(\xi_2 H)B_1', \\ &\sum_{n=0}^{\infty} a_n = A_1', \qquad \sum_{n=0}^{\infty} b_n = \frac{e_{15}'}{\varepsilon_{11}'}A_1' + B_1'. \end{aligned} \tag{23}$$

Non-trivial solutions can only exist when the determinant of the coefficient matrix of equation (23) is equal to zero, which yields the frequency equation of thickness-

Table 3. Values of P_{ij}.

	j			
i	3	4	5	6
5	−17 994 091 379 838.766	−2866 100 456 582.2344	22 710.925 588 1967	3614.581 280 0306
6	22 710.925 588 1967	3614.581 280 0306	−0.000 028 7672	−0.000 004 5785
7	−0.350 095 1655	0.485 729 4185	0.0	0.0
8	−211 655 413 144.116 73	−33 258 311 017.704 235	267.746 761 4837	42.612 923 3742

Table 4. Values of Q_{ij} ($n = 35$).

	j			
i	3	4	5	6
5	−17 994 091 379 838.715	−2866 100 456 582.2319	22 710.925 588 1967	3614.581 280 0306
6	22 710.925 588 1967	3614.581 280 0306	−0.000 028 7672	−0.000 004 5785
7	−0.350 095 1655	0.485 729 4185	0.0	0.0
8	−211 655 413 144.116 58	−33 258 311 017.704 224	267.746 761 4837	42.612 923 3742

twist wave propagation in the inhomogeneous piezoelectric plate [11, 29]

$$|Q_{ij}| = 0, \quad (i = 1, 2, 3, \ldots, 8;\ j = 1, 2, 3, \ldots, 8) \tag{24}$$

where

$$\begin{aligned}
Q_{11} &= -\bar{c}^*_{44}(\xi^*_1 H), \qquad Q_{12} = -e^*_{15}(\xi_2 H),\\
Q_{14} &= c^0_{44}, \qquad Q_{16} = e^0_{15}, \qquad Q_{22} = \varepsilon^*_{11}(\xi_2 H),\\
Q_{24} &= e^0_{15}, \qquad Q_{26} = -\varepsilon^0_{11}, \qquad Q_{31} = -1,\\
Q_{33} &= 1, \qquad Q_{41} = -\frac{e^*_{15}}{\varepsilon^*_{11}},\\
Q_{42} &= -1, \qquad Q_{45} = 1,\\
Q_{5k} &= \sum_{n=0}^{\infty}(n+1)[c^0_{44}(1-\alpha)a_{n+1} + e^0_{15}(1-\beta)b_{n+1}],\\
Q_{57} &= \bar{c}'_{44}(\xi'_1 H), \qquad Q_{58} = e'_{15}(\xi_2 H),\\
Q_{6k} &= \sum_{n=0}^{\infty}(n+1)[e^0_{15}(1-\beta)a_{n+1} - \varepsilon^0_{11}(1-\gamma)b_{n+1}],\\
Q_{68} &= -\varepsilon'_{11}(\xi_2 H), \qquad Q_{7k} = \sum_{n=0}^{\infty} a_n,\\
Q_{77} &= -1, \qquad Q_{8k} = \sum_{n=0}^{\infty} b_n,\\
Q_{87} &= -\frac{e'_{15}}{\varepsilon'_{11}}, \qquad Q_{88} = -1
\end{aligned} \tag{25}$$

in which $k = 3$–6 and all the other terms are equal to zero.

3. Numerical simulation and discussions

Equation (24) is a transcendental equation wherein frequency cannot be solved using an explicit expression. Thus, we adopt an iterative procedure for the numerical computations [33]. For an initial value of ω, we evaluate the determinant, which is presented in the left side of equation (24), for the various values of the unknown quantity. A fixed but small increment is added each time to this unknown quantity until the value of the determinant changes its sign. Then, the 'bisection method' is applied to locate the root correct to a chosen number of decimal places.

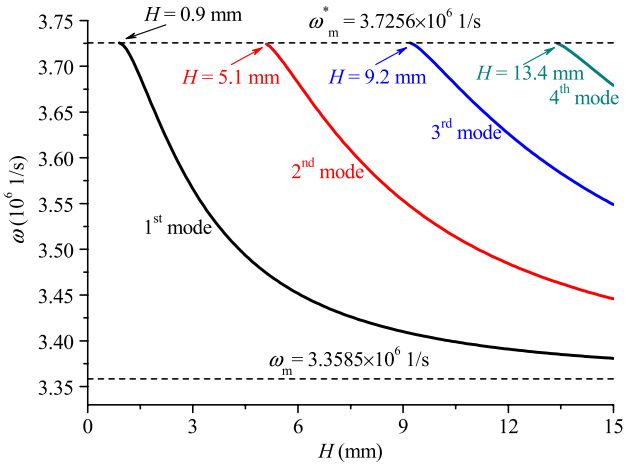

Figure 2. Frequency ω of different modes as a function of the length H of the middle layer when $\alpha = \beta = \gamma = \eta = 0$.

We take $h = 2$ mm and $m = 2$ as a numerical example. To study the thickness-twist waves in the structure and to show the effect of the functionally graded piezoelectric middle layer on the resonance frequency graphically, the following material system is considered: a semi-infinite PZT-5H in the left portion $x_1 < 0$ and PZT-4 in the right portion $x_1 > H$ [34, 35]. For PZT-5H, $c^*_{44} = 2.30 \times 10^{10}$ N m^{-2}, $e^*_{15} = 17.0$ C m^{-2}, $\varepsilon^*_{11} = 1.506 \times 10^{-8}$ C V^{-1} m^{-1}, and $\rho^* = 7500$ kg m^{-3}. For PZT-4, $c'_{44} = 2.56 \times 10^{10}$ N m^{-2}, $e'_{15} = 12.7$ C m^{-2}, $\varepsilon'_{11} = 6.46 \times 10^{-9}$ C V^{-1} m^{-1}, and $\rho' = 7500$ kg m^{-3}. Therefore, the corresponding cut-off frequencies are $\omega^*_{\mathrm{m}} = 3.7256 \times 10^6$ s^{-1} and $\omega'_{\mathrm{m}} = 4.0787 \times 10^6$ s^{-1}. For the trapped thickness-twist modes, we select PZT-7 for the non-graded piezoelectric middle layer, i.e., $c^0_{44} = 2.50 \times 10^{10}$ N m^{-2}, $e^0_{15} = 13.5$ C m^{-2}, $\varepsilon^0_{11} = 1.71 \times 10^{-8}$ C V^{-1} m^{-1}, $\rho^0 = 7800$ kg m^{-3}, and $\omega_{\mathrm{m}} = 3.3585 \times 10^6$ s^{-1} [34, 35].

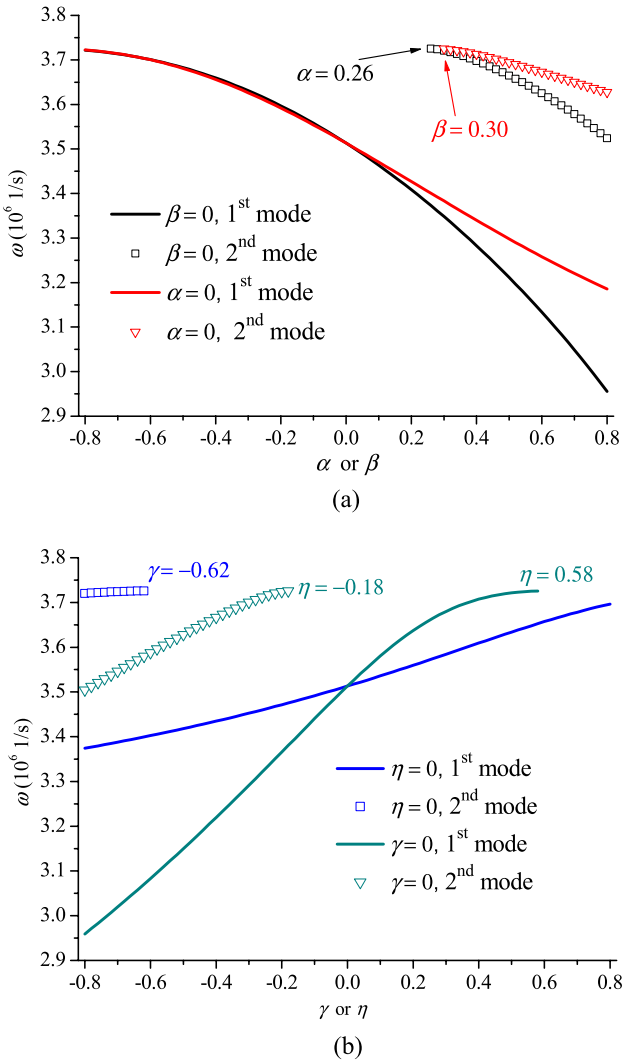

Figure 3. Frequency ω with different graded coefficients ($H = 4$ mm): (a) α or β shifts ($\gamma = \eta = 0$); (b) γ or η shifts ($\alpha = \beta = 0$).

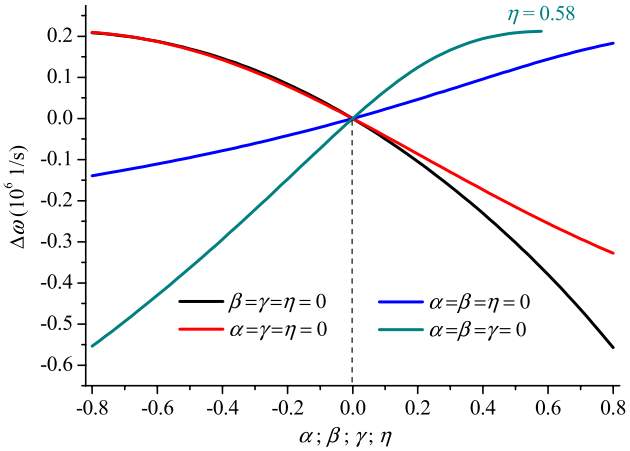

Figure 4. Frequency shift $\Delta\omega$ attributed to the graded middle layer with different graded coefficients.

3.1. Convergence of the power series

First, we examined the convergence of the series. Tables 1 and 2 show the frequencies of the plate for some special

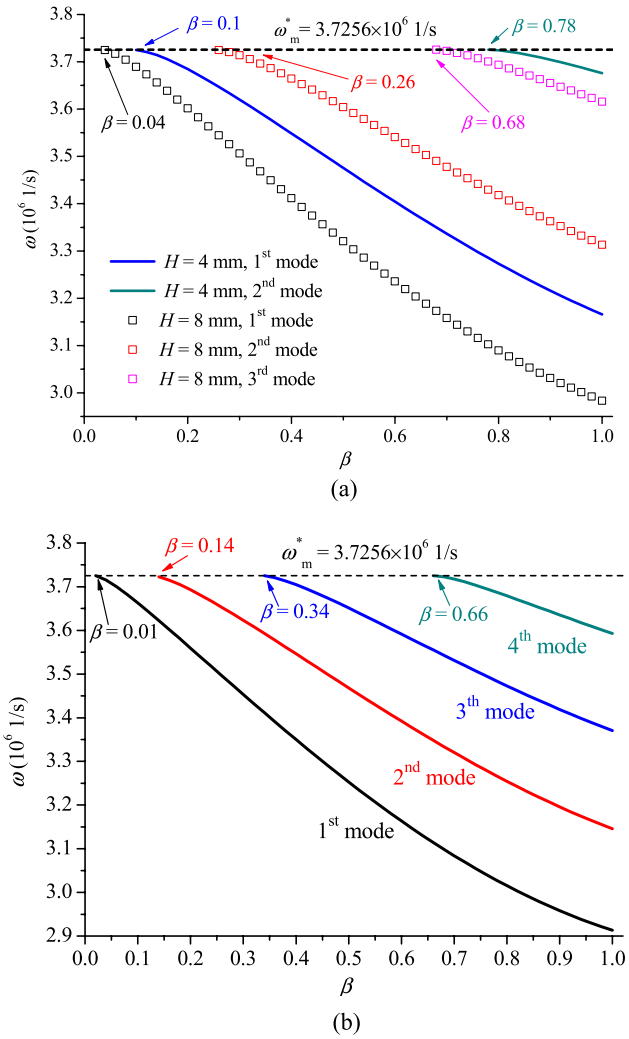

Figure 5. Frequency ω of different modes as a function of the left damaged parameter β for some selected H: (a) $H = 4$ and 8 mm; (b) $H = 12$ mm.

cases using the power function expansion method. The change of graded parameters α, β, γ, and η does not affect the convergence of this series, which can be obtained from table 2. However, the numerical precision is closely related to the length H, which can be obtained from table 1. In the present text, the length of graded middle layer is no more than 15 mm, therefore 100 terms in the series are sufficient to ensure acceptable accuracy in the following simulation.

3.2. Verification of the power series

Second, we compared the results calculated using the power function expansion method with the theoretical results to correct the power series. For the homogeneous middle layer, i.e., $\alpha = \beta = \gamma = \eta = 0$, the theoretical solutions can easily be derived as [20]

$$u = [A_1 \cos(\xi_1 x_1) + A_2 \sin(\xi_1 x_1)] \cos(\xi_2 x_2) \exp(-\mathrm{i}\omega t)$$

$$\varphi = \begin{cases} \dfrac{e_{15}^0}{\varepsilon_{11}^0} [A_1 \cos(\xi_1 x_1) + A_2 \sin(\xi_1 x_1)] \end{cases}$$

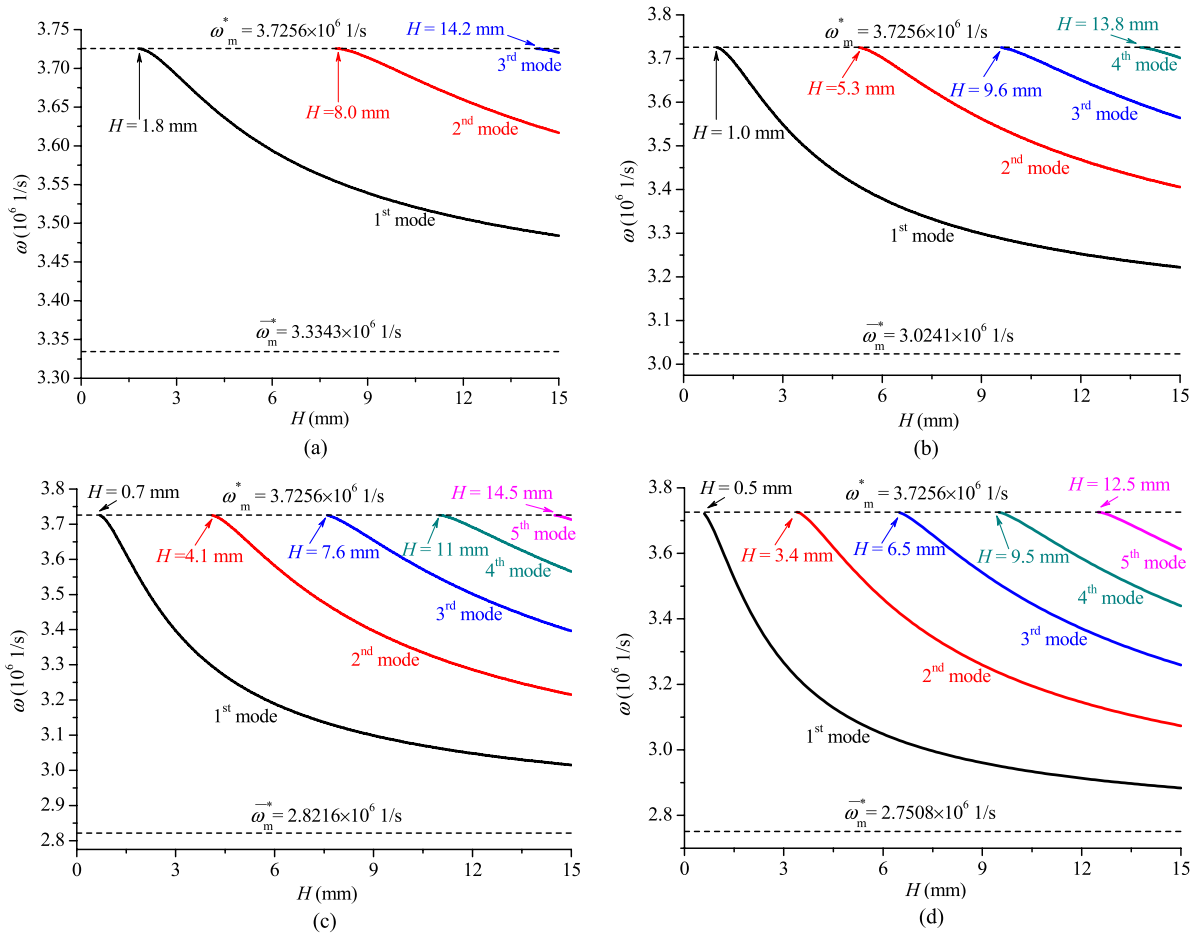

Figure 6. Frequency ω of different modes as a function of the damaged length H of the left material for some selected piezoelectric graded coefficients β: (a) $\beta = 0.25$; (b) $\beta = 0.50$; (c) $\beta = 0.75$; and (d) $\beta = 1.0$.

$$\left.\begin{aligned} &+ [B_1 \cosh(\xi_2 x_1) + B_2 \sinh(\xi_2 x_1)] \Big\} \\ &\times \cos(\xi_2 x_2) \exp(-\mathrm{i}\omega t) \end{aligned}\right. \tag{26}$$

$$\begin{aligned} T_{31} &= \{\bar{c}^0_{44}\xi_1[-A_1 \sin(\xi_1 x_1) + A_2 \cos(\xi_1 x_1)] \\ &\quad + e^0_{15}\xi_2[B_1 \sinh(\xi_2 x_1) + B_2 \cosh(\xi_2 x_1)]\} \\ &\quad \times \cos(\xi_2 x_2) \exp(-\mathrm{i}\omega t) \\ D_1 &= -\varepsilon^0_{11}\xi_2[B_1 \sinh(\xi_2 x_1) \\ &\quad + B_2 \cosh(\xi_2 x_1)] \cos(\xi_2 x_2) \exp(-\mathrm{i}\omega t). \end{aligned} \tag{27}$$

Similarly, substituting equations (4), (6), (8), (10), (26), and (27) into the continuity condition equation (21) yields eight linear, homogeneous algebraic equations for coefficients A^*_1, B^*_1, A_1, A_2, B_1, B_2, A'_1, and B'_1:

$$\begin{aligned} &\bar{c}^*_{44}\xi^*_1 A^*_1 + e^*_{15}\xi_2 B^*_1 = \bar{c}^0_{44}\xi_1 A_2 + e^0_{15}\xi_2 B_2, \\ &-\varepsilon^*_{11}\xi_2 B^*_1 = -\varepsilon^0_{11}\xi_2 B_2, \qquad A^*_1 = A_1, \\ &\frac{e^*_{15}}{\varepsilon^*_{11}} A^*_1 + B^*_1 = \frac{e^0_{15}}{\varepsilon^0_{11}} A_1 + B_1, \\ &\bar{c}^0_{44}\xi_1[-A_1 \sin(\xi_1 H) + A_2 \cos(\xi_1 H)] \\ &\quad + e^0_{15}\xi_2[B_1 \sinh(\xi_2 H) + B_2 \cosh(\xi_2 H)] \\ &\quad = -\bar{c}'_{44}\xi'_1 A'_1 - e'_{15}\xi_2 B'_1, \\ &-\varepsilon^0_{11}\xi_2[B_1 \sinh(\xi_2 H) + B_2 \cosh(\xi_2 H)] = \varepsilon'_{11}\xi_2 B'_1, \\ &A_1 \cos(\xi_1 H) + A_2 \sin(\xi_1 H) = A'_1, \\ &\frac{e^0_{15}}{\varepsilon^0_{11}}[A_1 \cos(\xi_1 H) + A_2 \sin(\xi_1 H)] + [B_1 \cosh(\xi_2 H) \\ &\quad + B_2 \sinh(\xi_2 H)] = \frac{e'_{15}}{\varepsilon'_{11}} A'_1 + B'_1. \end{aligned} \tag{28}$$

Non-trivial solutions can exist only when the determinant of the coefficient matrix of equation (28) is equal to zero. To maintain alignment with equation (23), we transformed some rows of the coefficient matrix to determine the frequency equation for the non-graded middle layer:

$$\begin{aligned} &|P_{ij}| = 0, \\ &\quad (i = 1, 2, 3, \ldots, 8;\ j = 1, 2, 3, \ldots, 8) \end{aligned} \tag{29}$$

where

$$\begin{aligned} &P_{11} = -\bar{c}^*_{44}(\xi^*_1 H), \qquad P_{12} = -e^*_{15}(\xi_2 H), \\ &P_{14} = c^0_{44}, \qquad P_{16} = e^0_{15}, \\ &P_{22} = \varepsilon^*_{11}(\xi_2 H), \qquad P_{24} = e^0_{15}, \qquad P_{26} = -\varepsilon^0_{11}, \\ &P_{31} = -1, \qquad P_{33} = 1, \\ &P_{41} = -\frac{e^*_{15}}{\varepsilon^*_{11}}, \qquad P_{42} = -1, \qquad P_{45} = 1, \end{aligned}$$

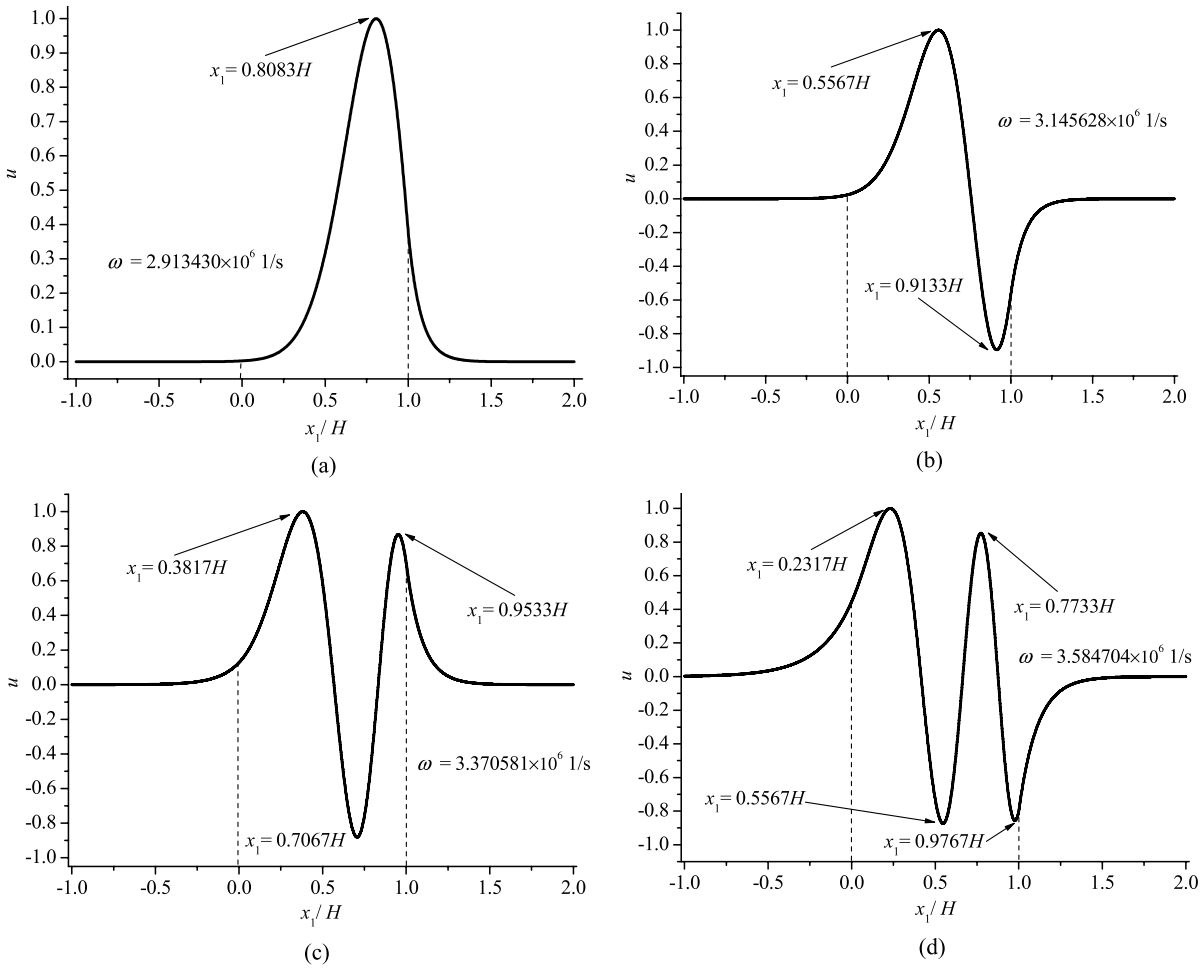

Figure 7. Relative displacement component u of different modes along the x_1 direction at $x_2 = 0$ for left material damage when $H = 12$ mm and $\beta = 1$: (a) first mode ($\omega = 2.913\,430 \times 10^6$ s^{-1}); (b) second mode ($\omega = 3.145\,628 \times 10^6$ s^{-1}); (c) third mode ($\omega = 3.370\,581 \times 10^6$ s^{-1}); and (d) fourth mode ($\omega = 3.584\,704 \times 10^6$ s^{-1}).

$$
\begin{aligned}
P_{53} &= -\bar{c}^0_{44}(\xi_1 H)\sin(\xi_1 H) - \frac{e^{0\,2}_{15}}{\varepsilon^0_{11}}(\xi_2 H)\sinh(\xi_2 H),\\
P_{54} &= \bar{c}^0_{44}\cos(\xi_1 H) - \frac{e^{0\,2}_{15}}{\varepsilon^0_{11}}\cosh(\xi_2 H),\\
P_{55} &= e^0_{15}(\xi_2 H)\sinh(\xi_2 H),\\
P_{56} &= e^0_{15}\cosh(\xi_2 H),\\
P_{57} &= \bar{c}'_{44}(\xi'_1 H), \qquad P_{58} = e'_{15}(\xi_2 H),\\
P_{63} &= e^0_{15}(\xi_2 H)\sinh(\xi_2 H),\\
P_{64} &= e^0_{15}\cosh(\xi_2 H),\\
P_{65} &= -\varepsilon^0_{11}(\xi_2 H)\sinh(\xi_2 H),\\
P_{66} &= -\varepsilon^0_{11}\cosh(\xi_2 H), \qquad P_{68} = -\varepsilon'_{11}(\xi_2 H),\\
P_{73} &= \cos(\xi_1 H), \qquad P_{74} = \frac{\sin(\xi_1 H)}{\xi_1 H},\\
P_{75} &= P_{76} = 0, \qquad P_{77} = -1,\\
P_{83} &= \frac{e^0_{15}}{\varepsilon^0_{11}}[\cos(\xi_1 H) - \cosh(\xi_2 H)],\\
P_{84} &= \frac{e^0_{15}}{\varepsilon^0_{11}}\left[\frac{\sin(\xi_1 H)}{\xi_1 H} - \frac{\sinh(\xi_2 H)}{\xi_2 H}\right],\\
P_{85} &= \cosh(\xi_2 H),\\
P_{86} &= \frac{\sinh(\xi_2 H)}{\xi_2 H}, \qquad P_{87} = -\frac{e'_{15}}{\varepsilon'_{11}},\\
P_{88} &= -1.
\end{aligned}
\tag{30}
$$

All other components of P_{ij} are equal to zero. Comparing equation (30) with (25), we find that $\boldsymbol{P}$ and $\boldsymbol{Q}$ have the same expression, except for P_{ij} and Q_{ij} ($i = 5$–8, $j = 3$–6). Tables 3 and 4 respectively provide the values of P_{ij} and Q_{ij} when $H = 4$ mm. P_{ij} is calculated using the theoretical solution, whereas Q_{ij} is obtained using the power function expansion method. The values are almost the same even for a few relative terms, as shown in tables 3 and 4. This condition indicates that the power series has high precision and can be used to solve the propagation of thickness-twist waves in a functionally graded piezoelectric plate.

3.3. Effect of graded coefficient on resonance frequency

Numerical analysis results show the basic properties of thickness-twist wave propagation in the inhomogeneous plate. The variation pattern of frequency ω as a function of the

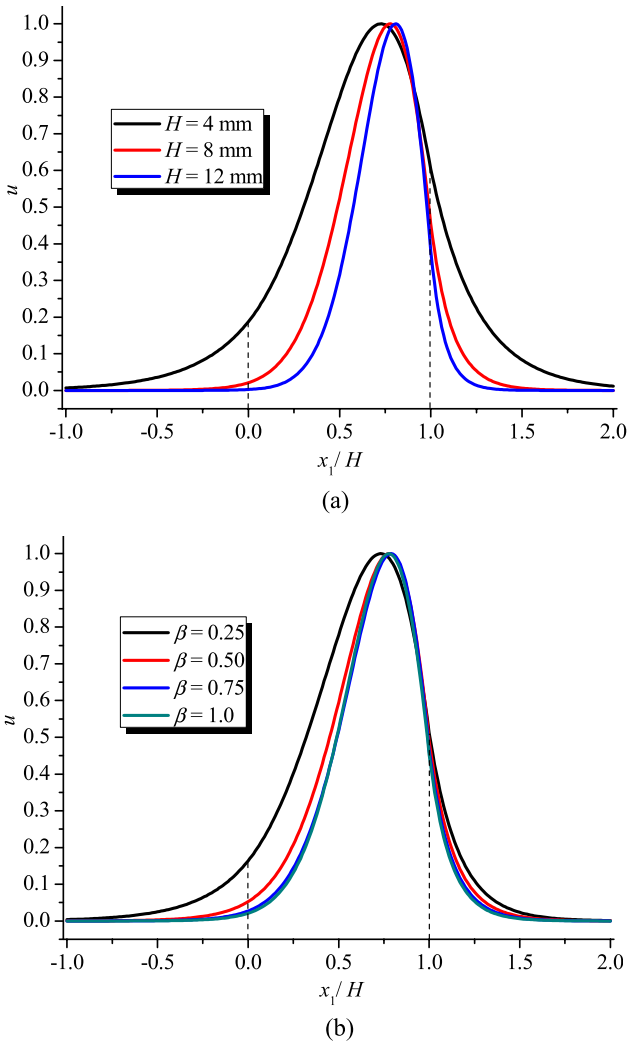

Figure 8. Relative displacement component u of fundamental mode along the x_1 direction at $x_2 = 0$ for some selected H and β under left material damage: (a) for some selected H and (b) for some selected β.

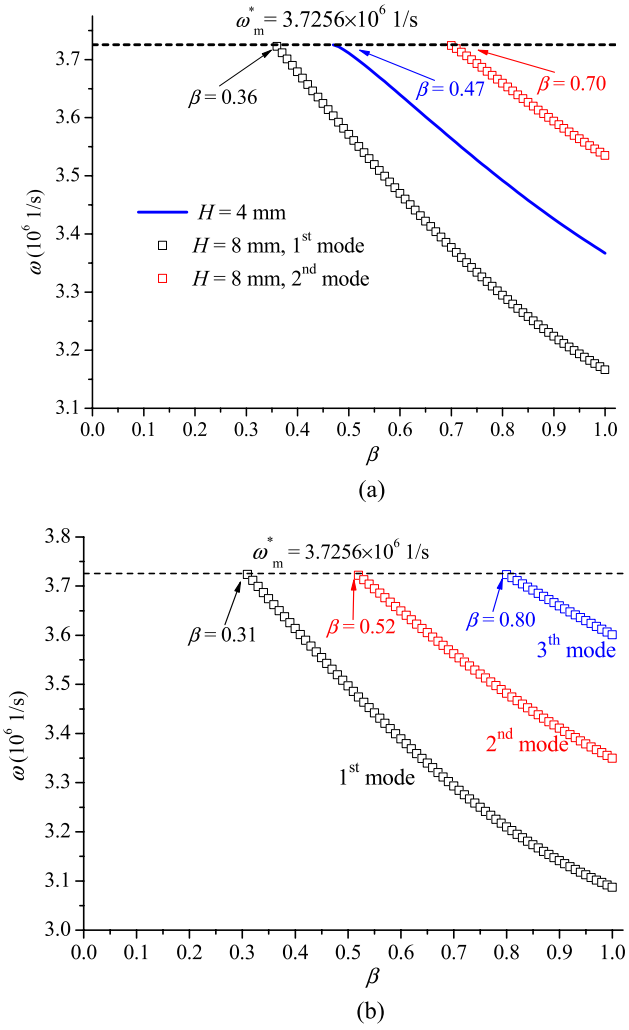

Figure 9. Frequency ω of different modes as a function with the right damaged parameter β for some selected H: (a) $H = 4$ and 8 mm; (b) $H = 12$ mm.

length H of the middle layer when $\alpha = \beta = \gamma = \eta = 0$, i.e., the homogeneous middle layer, is shown in figure 2. The frequencies of all the trapped modes initiate at the cut-off frequency of the left region ω_m^* and approach the cut-off frequency of the non-graded middle layer ω_m as the length H increases. In device applications, H is an important parameter for determining Bechmann's number [36], which is related to the ratio of the plate thickness and length when only one trapped mode exists in the plate. On one hand, the first mode exists only when the length achieves some value, i.e., $H \geq 0.9$ mm. On the other hand, the modes appear periodically at approximately $\Delta H = 4.2$ mm. For instance, the first mode appears at $H = 0.9$ mm, the second at $H = 5.1$ mm, the third at $H = 9.2$ mm, and the fourth at $H = 13.4$ mm. This phenomenon is explained by equation (30), which contains the periodical terms, such as the sin and cos functions, in P_{ij} ($i = 5$–8, $j = 3$–6). The power series is as precise as the theoretical results, which leads to the periodic appearance of the modes.

We next investigate the effect of graded coefficients on the thickness-twist wave propagation. We assume that the piezoelectric coefficient, dielectric permittivity, and mass density of the middle layer are homogeneous, i.e., $\beta = \gamma = \eta = 0$, when we focus on the effect of the elastic coefficient. The same method can be used in addressing the piezoelectric coefficient, dielectric permittivity, and mass density. Figure 3 presents the resonance frequency with the change of the graded parameter as α, β, γ, and η, respectively. Changes in the material coefficient increase or decrease the number of trapped modes. For example, only one mode exists for the homogeneous layer $H = 4$ mm. The reduction of the elastic and piezoelectric coefficients, i.e., the increase in the values of α and β, enables higher modes to appear but reduces resonance frequency. However, dielectric permittivity and mass density have opposite effects especially because no trapped modes exist when $\eta > 0.58$.

To study the effect of the graded parameter on wave propagation further, the frequency shift is defined as $\Delta\omega = \omega - \omega_0$, where ω is the frequency of the plate when only one material parameter changes, and ω_0 represents the

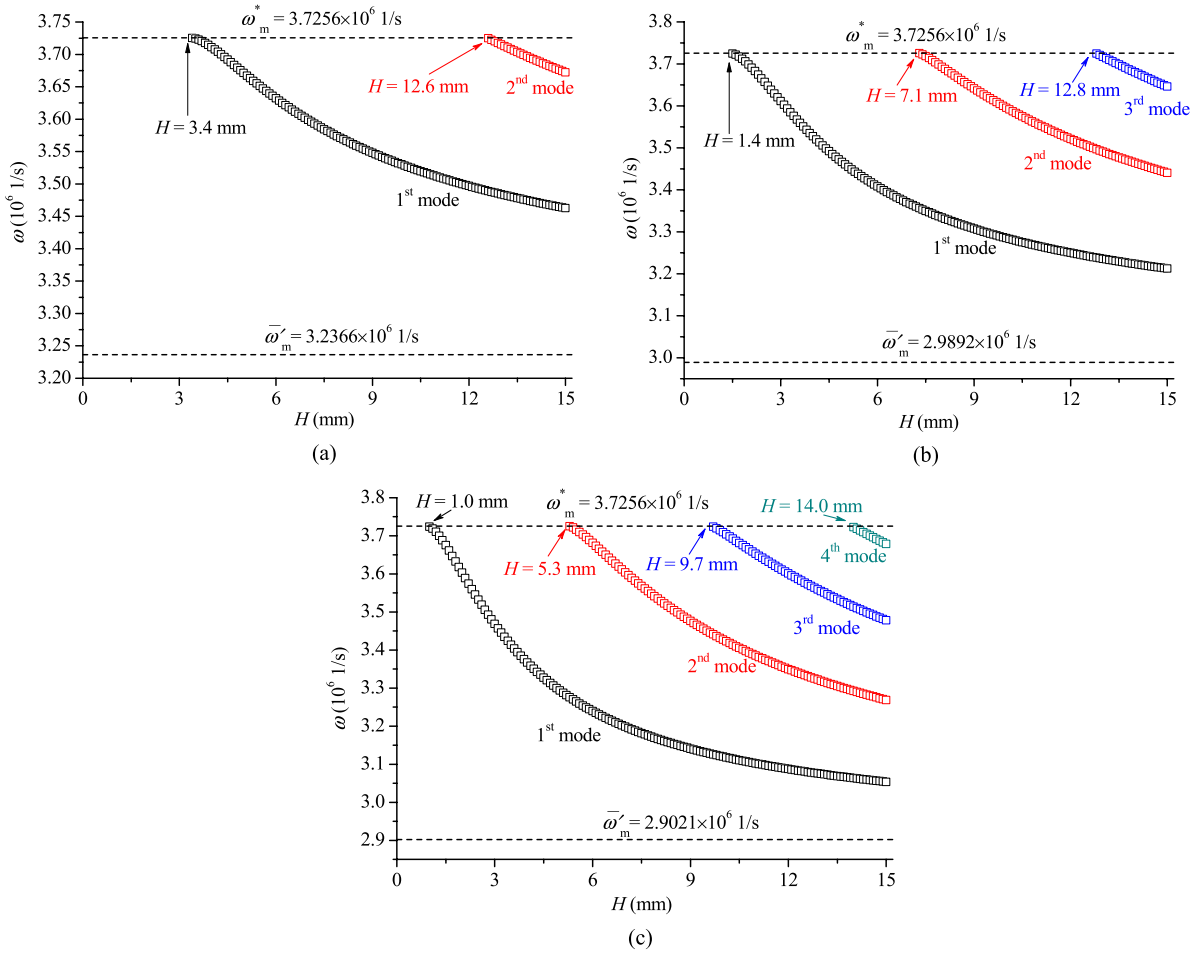

Figure 10. Frequency ω of different modes as a function of the damaged length of the right material H for some selected damage parameters β: (a) $\beta = 0.50$; (b) $\beta = 0.75$; and (c) $\beta = 1.0$.

frequency of the plate with the non-graded middle layer. The frequency shift $\Delta\omega$ attributed to the graded middle layer with different graded coefficients α, β, γ, or η is shown in figure 4 for comparison. The increase in elastic and piezoelectric parameters decelerates the thickness-twist wave, whereas the increase in dielectric permittivity and mass density hastens its propagation. The effect of the elastic coefficient is more evident than that of the piezoelectric constant. The absolute value of the frequency shift attributed to the change in mass density is larger than that attributed to dielectric permittivity. These conclusions can be used to estimate the effects of graded coefficients and of the thickness-twist wave characteristics on the functionally graded piezoelectric plate.

4. The trapped modes attributed to piezoelectric damage

Defect during material manufacture as well as a corrosive environment and fatigue under periodic mechanical or thermal loading during device operation usually result in material damage to the piezoelectric wafer. For instance, a small flaw or hole may exist in the plate during the production or the piezoelectric damage phenomenon may occur near the bonding interface during device application [5]. Given that such a flaw or hole has faint effects, this kind of fault and piezoelectric damage does not affect the elastic, dielectric, and density properties of materials. However, the piezoelectric coefficient may change, which makes the plate inhomogeneous. In this section, we investigate the effect of FGPM on thickness-twist waves that can be attributed to the piezoelectric damage that occurs at the interface, i.e., $\alpha = \gamma = \eta = 0$ and $\beta \neq 0$.

4.1. Piezoelectric damage attributed to the left region material

The functionally graded middle layer is assumed to occur because of piezoelectric damage to the left region material $x_1 < 0$, i.e., $c^0_{44} = c^*_{44}$, $e^0_{15} = e^*_{15}$, $\varepsilon^0_{11} = \varepsilon^*_{11}$, $\rho^0 = \rho^*$, where H is the damage length. Considering that the piezoelectric coefficient can be zero, β changes from 0 to 1. Figures 5 and 6 respectively show the frequency ω of different modes as a function of the piezoelectric graded coefficient β and the damaged length H in some special cases.

Figures 5 and 6 also show that all frequencies of trapped modes initiate the cut-off frequency of the left region material ω^*_m, and both the piezoelectric graded coefficient β and damaged length H reduce resonance

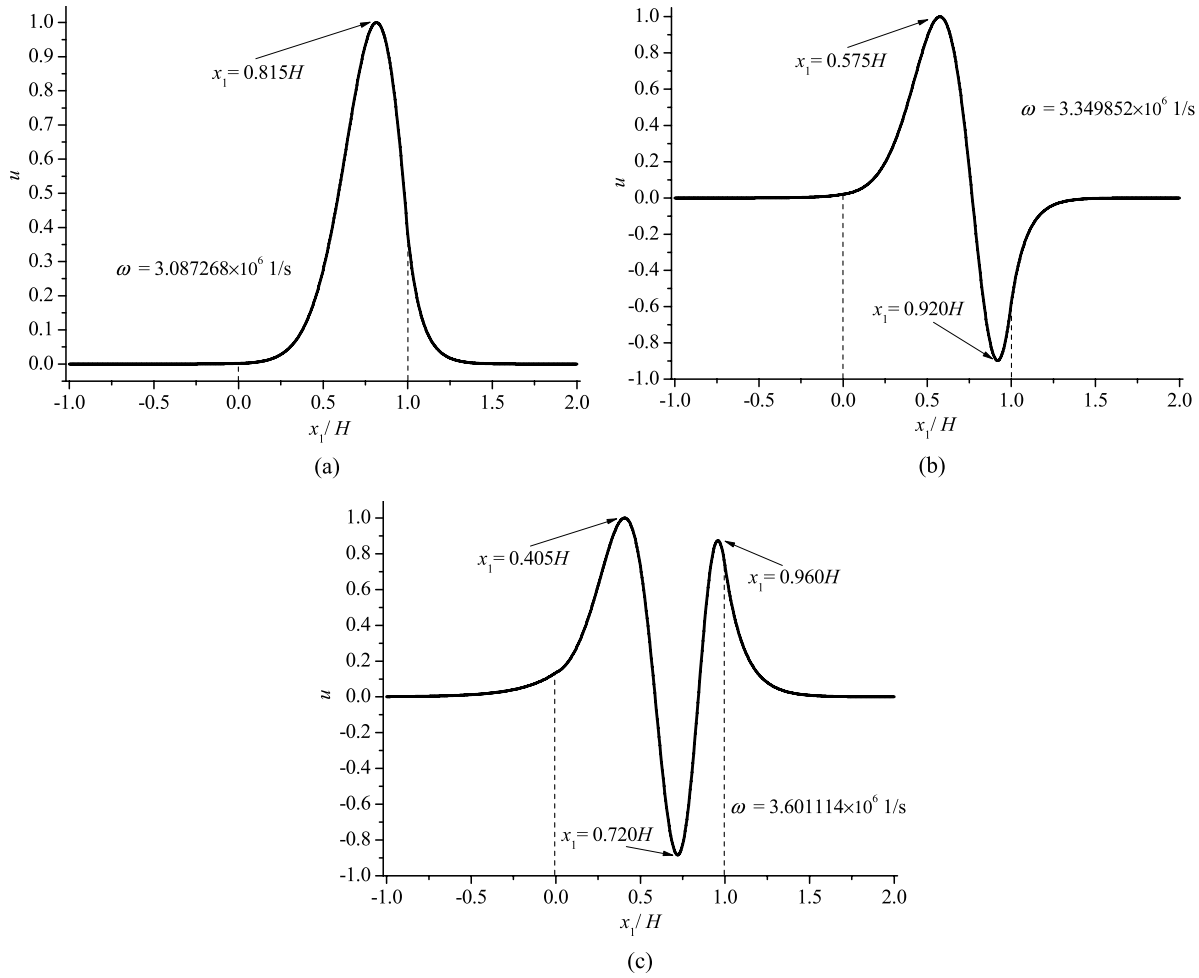

Figure 11. Relative displacement component u of different modes along the x_1 direction at $x_2 = 0$ for right material damage when $H = 12$ mm and $\beta = 1$: (a) first mode ($\omega = 3.087\,268 \times 10^6$ s^{-1}); (b) second mode ($\omega = 3.349\,852 \times 10^6$ s^{-1}); and (c) third mode ($\omega = 3.601\,114 \times 10^6$ s^{-1}).

frequency. For convenience, we define $\bar{\omega}^*_{\mathrm{m}} = (\frac{m\pi}{2h})\bar{c}^*_{\mathrm{sh}} = (\frac{m\pi}{2h})\sqrt{\frac{1}{\rho^*}[c^*_{44} + \frac{e^{*2}_{15}(1-\beta)^2}{\varepsilon^*_{11}}]}$ as the limit cut-off frequency for the left material with piezoelectric damage, which is the lower limit of the frequencies.

No piezoelectric damage, i.e., $H = 0$ or $\beta = 0$, indicates that no modes are trapped in the plate, as shown in figures 5 and 6. Therefore, the piezoelectric damage facilitates the energy-trapping phenomenon. Increasing values of β and H result in an increase in the number of the trapped modes. Comparing figures 5 and 6, we can conclude that the higher modes appear periodically with increasing damaged length H. In the case of $\beta = 0.25$, the period is $\Delta H = 6.8$ mm; for $\beta = 0.50$, ΔH is approximately 4.3 mm; for $\beta = 0.75$, $\Delta H = 3.5$ mm; and for $\beta = 1.0$, $\Delta H = 3$ mm. The expansion of the damaged length leads to the earlier appearance of new modes. However, this kind of periodic characteristic does not exist with the increase in piezoelectric parameter β.

Four modes exist when $H = 12$ mm and $\beta = 1$, as shown in figure 6(d). Figure 7 gives the relative displacement component of these modes along the x_1 direction at $x_2 = 0$ when $A^*_1 = 1$ m. The value of the displacement component is normalized such that the maximal displacement at the damage layer is equal to one [37]. Therefore, the displacement u in figure 7 is a physically non-dimensional number. The value is nearly zero when $x_1 > 1.5H$ or $x_1 < -0.5H$, which suggests that the energy mainly concentrates on the region of $-0.5H \leq x_1 \leq 1.5H$, which explains 'energy trapping'. Given the inhomogeneous damaged layer, the displacement is neither symmetric nor anti-symmetric at approximately $x_1 = 0$, which differs from that of the homogeneous middle layer. For example, the maximum displacement of the fundamental mode occurs at $x_1 = 0.8083H$ in the damaged plate, not at $x_1 = 0.50H$. Comparing the value of displacement at $x_1 = 0$ and H, we can deduce that the thickness-twist waves trap faster at the left region.

We present the relative displacement distribution of the fundamental mode to compare the effects of the damaged parameter β and the damaged length H on the amplitude of resonance. This distribution is the usual operating mode of a resonator and is widely used in device applications as in figure 8, which shows that a larger damaged length H and parameter β trap more energy in the damaged region.

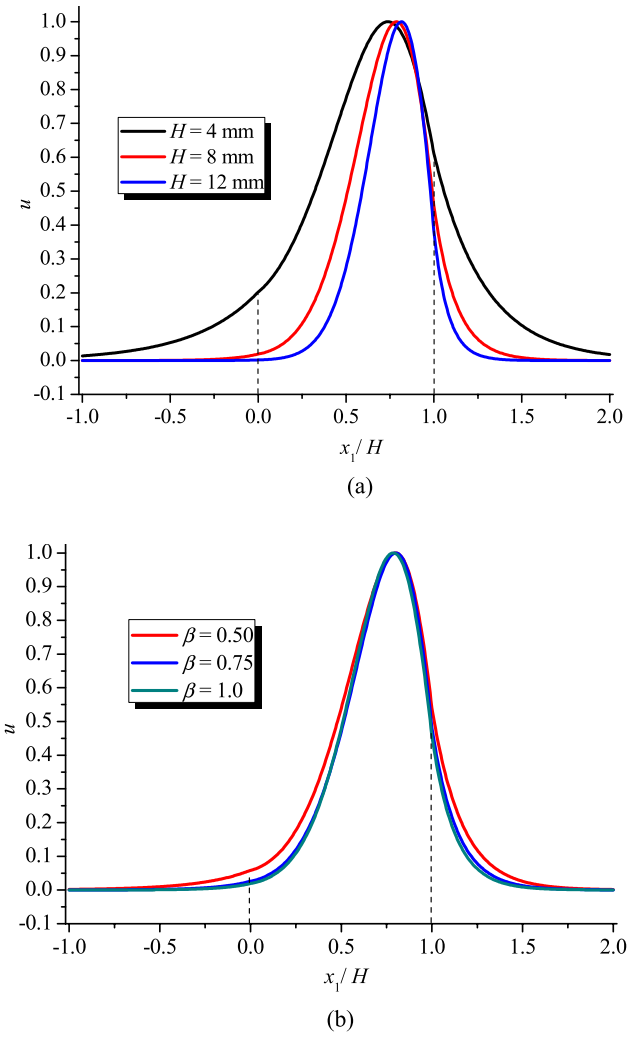

Figure 12. Relative displacement component u of fundamental mode along the x_1 direction at $x_2 = 0$ for some selected H and β under right material damage: (a) for some selected H and (b) for some selected β.

4.2. Piezoelectric damage attributed to the right region material

Similarly, we assume that the functionally graded middle layer occurs because of the piezoelectric damage of right region material $x_1 > H$, which means $c_{44}^0 = c'_{44}, e_{15}^0 = e'_{15}, \varepsilon_{11}^0 = \varepsilon'_{11}, \rho^0 = \rho'$, and H is the damaged length. The same parameter $\bar{\omega}'_{\mathrm{m}} = (\frac{m\pi}{2h})\bar{c}'_{\mathrm{sh}} = (\frac{m\pi}{2h})\sqrt{\frac{1}{\rho'}[c'_{44} + \frac{e'^2_{15}(1-\beta)^2}{\varepsilon'_{11}}]}$ can be defined as the limit cut-off frequency for the right material with piezoelectric damage. Figures 9 and 10 give the frequency ω of different modes as a function of the right damaged parameter β for some selected H and with damaged length H for some damage parameter β, respectively. All the frequencies of the trapped modes also initiate the cut-off frequency of the left portion material ω^*_{m}. Furthermore, the increasing of β and H expectedly increases the number of modes but reduces the resonance frequency. The higher modes also appear periodically with H, but the period is longer than that for left material damage. The effect of left material damage on thickness-twist waves is more evident than that of right material damage. On one hand, the number of modes is greater than that with right material damage. For example, five modes exist in $\beta = 1$ as shown in figure 6(d), but only four modes exist when the right material is damaged as shown in figure 10(c). No modes exist for $\beta = 0.25$ in this case. On the other hand, right material damage facilitates the later appearance of a higher mode compared with left material damage. For instance, the fundamental mode emerges until $\beta = 0.47$ when $H = 4$ mm, which can be seen from figure 10(a). However, the value is 0.10 under the same conditions.

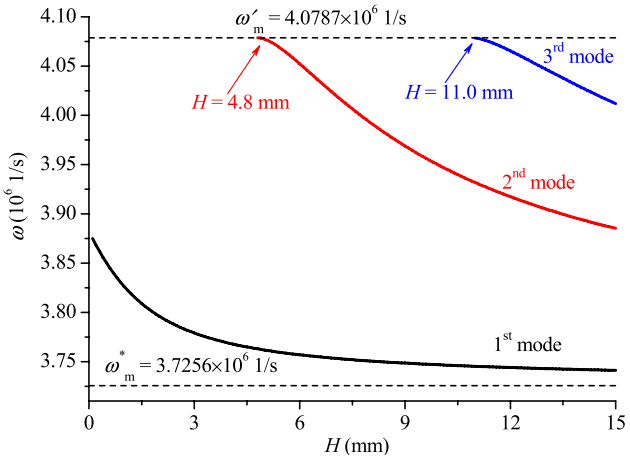

Figure 13. The frequency ω of different modes as a function with the length H of the transition layer.

We can forecast the left material piezoelectric damage in some particular frequency spectrum ranges based on the change of resonance frequency when the plate is damaged. In figures 6(d) and 10(c) for instance, $\bar{\omega}^*_{\mathrm{m}} = 2.7508\times10^6\ \mathrm{s}^{-1}$ and $\bar{\omega}'_{\mathrm{m}} = 2.9021\times10^6\ \mathrm{s}^{-1}$ for $\beta = 1.0$. Therefore, the damaged region is $x_1 < 0$ if the frequency satisfies $\bar{\omega}^*_{\mathrm{m}} < \omega < \bar{\omega}'_{\mathrm{m}}$.

Given the inhomogeneous damage layer, the displacement is neither symmetric nor anti-symmetric at approximately $x_1 = 0$, as shown in figure 11, which is similar to figure 7. Greater damaged length H and parameter β trap more energy in the damage region as shown in figure 12.

In conclusion, left or right piezoelectric material damage facilitates the energy trapping, which is impossible for perfect materials. With the increase in piezoelectric damaged length and the reduction of the piezoelectric coefficient, the resonance frequency decreases but higher modes of thickness-twist waves appear. The modes periodically appear along the damage length. Moreover, the displacement is neither symmetric nor anti-symmetric at approximately the center of the damaged portion, which differs from the non-graded plate.

5. FGPM transition layer between left and right piezoelectric materials

From the perspective of material manufacture, an FGPM can sometimes be designed as a buffer layer to avoid the

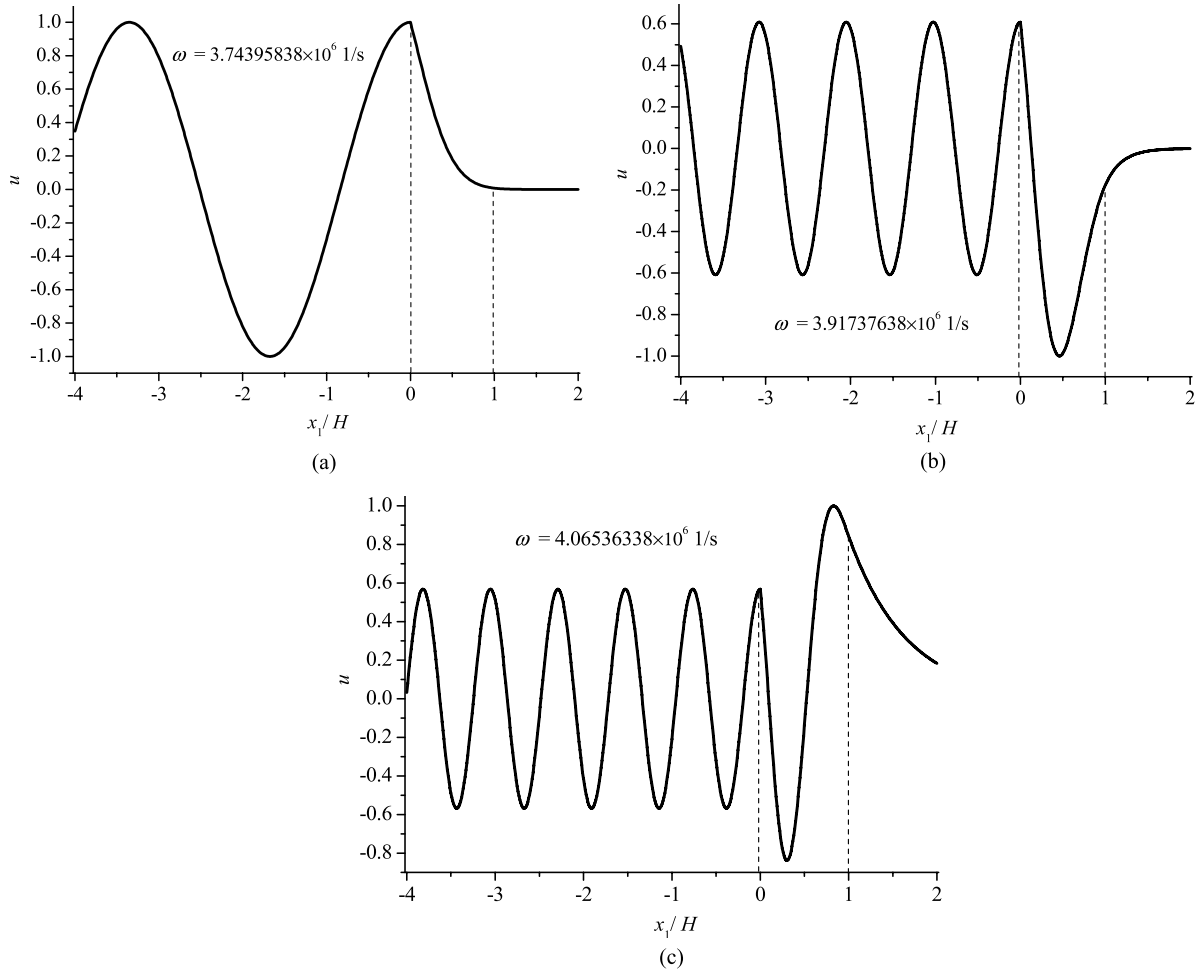

Figure 14. Relative displacement component u of different modes along the x_1 direction at $x_2 = 0$ with the transition layer length $H = 12$ mm: (a) first mode ($\omega = 3.743\,958\,38 \times 10^6$ s^{-1}); (b) second mode ($\omega = 3.917\,376\,38 \times 10^6$ s^{-1}); and (c) third mode ($\omega = 4.065\,363\,38 \times 10^6$ s^{-1}).

stress discontinuity of the interface [38]. Furthermore, the material characteristics in the neighborhood of the bonding interface must be influenced by two different materials if these materials have been bonded for a long time. A transition FGPM layer exists physically, thus changing the middle layer smoothly and steadily. In this paper, we assume that the FGPM middle layer in figure 1 is such a buffer layer, which indicates $c^0_{44} = c^*_{44}$, $e^0_{15} = e^*_{15}$, $\varepsilon^0_{11} = \varepsilon^*_{11}$, and $\rho^0 = \rho^*$ at $x_1 = 0$, whereas $c^0_{44}(1-\alpha) = c'_{44}$, $e^0_{15}(1-\beta) = e'_{15}$, $\varepsilon^0_{11}(1-\gamma) = \varepsilon'_{11}$, and $\rho^0(1-\eta) = \rho'$ at $x_1 = H$. We continue to adopt the same materials above, and the graded parameters can be calculated as $\alpha = -0.1130$, $\beta = 0.2529$, $\gamma = 0.5710$, and $\eta = 0$.

The resonance frequencies of the higher modes comprise the initial cut-off frequency ω'_{m} of the right region but the fundamental mode is not, and all modes approach the cut-off frequency ω^*_{m} of the left region, as shown in figure 13. Moreover, the wave is not fully completely trapped modes. For instance, figures 14 and 15 show that the amplitude of relative displacement does not approach zero at the left region $x_1 < 0$, which can be attributed to the fact that the resonance frequency ω is larger than ω^*_{m} and that the wave is harmonic without exponential attenuation. At the right region $x_1 < H$, the wave decays to zero because $\omega < \omega^*_{\mathrm{m}}$, and the lower modes attenuate faster than the higher ones. A larger transition length makes this kind of attenuation more evident and has a significant effect on the displacement component in the left region $x_1 < 0$.

6. Conclusions

In summary, the power-series technique was used to solve the propagation governing equation of a thickness-twist wave in an inhomogeneous plate with an FGPM middle layer in the center portion. The good convergence and high precision of these series have been illustrated. Some numerical examples were provided to illustrate the detailed effect of the graded factors on the frequencies and the displacement components of the thickness-twist waves in a structure (figure 1), which yields the following points:

- Graded factors significantly affect the characteristics of thickness-twist waves, not only in terms of the value of resonance frequencies but also the number of trapped modes. The waves propagate slowly, and higher modes

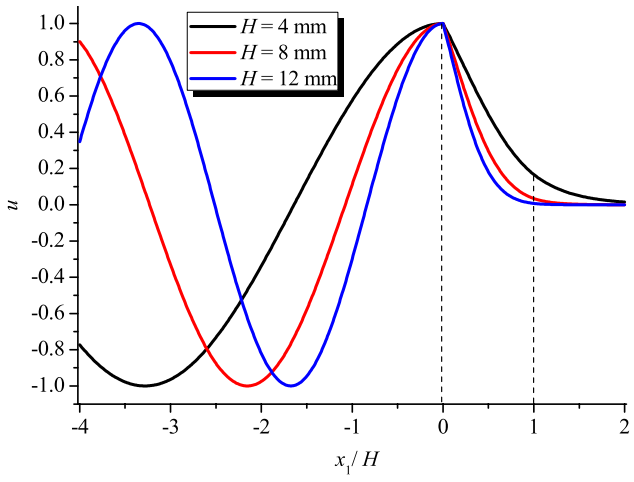

Figure 15. Relative displacement component u of fundamental mode along the x_1 direction at $x_2 = 0$ for some selected transition length H.

appear earlier with the reduction of the elastic and piezoelectric coefficients. Moreover, the effect of the dielectric permittivity and the mass density are opposites.

- Left or right piezoelectric material damage facilitates energy trapping, which is impossible for perfect materials. With increasing piezoelectric damaged length and decreasing piezoelectric coefficient, the resonance frequency decreases but higher modes of thickness-twist waves appear. The modes emerge periodically along the damaged length. Furthermore, the displacement is not symmetric at approximately the center of the damaged portion, which differs from the non-graded plate.
- In an FGPM transition layer, this wave is not characterized by completely trapped modes, which is only trapped in one region but propagate in the other portion.

The power-series expansion method applied in the present this paper could be used in the study of acoustic waves along with other analogous systems with inhomogeneous materials. Therefore, the piezoelectric damage that facilitates energy trapping can be used theoretically in the design of wave propagation in piezoelectric coupled structures.

Acknowledgments

The National Natural Science Foundation of China (Nos. 11272247 and 10902079), the National 111 Project of China (No. B06024), and the Scholarship Award for Excellent Doctoral Student granted by Ministry of Education are gratefully acknowledged for their financial support.

References

[1] Mindlin R D 1965 Thickness-twist vibrations of an infinite, monoclinic, crystal plate *Int. J. Solids Struct.* **1** 141–5
[2] Pearman G T 1969 Thickness-twist vibrations in beveled AT-cut quartz plates *J. Acoust. Soc. Am.* **45** 928–34
[3] Tiersten H F 1963 Wave propagation in an infinite piezoelectric plate *J. Acoust. Soc. Am.* **35** 234–9
[4] Tiersten H F, Lwo B J and Dulmet B 1996 Transversely varying thickness modes in trapped energy resonators with shallow and beveled contours *J. Appl. Phys.* **80** 1037–46
[5] Yang J, Chen Z and Hu Y 2007 Propagation of thickness-twist waves through a joint between two semi-infinite piezoelectric plates *IEEE Trans. Ultrason. Ferroelectr. Freq. Control* **54** 888–91
[6] Yang J, Chen Z, Hu Y, Jiang S and Guo S 2007 Propagation of thickness-twist waves in a multi-sectioned piezoelectric plate of 6 mm crystals *Arch. Appl. Mech.* **77** 689–96
[7] Erdogan F and Wu B H 1996 Crack problems in FGM layers under thermal stresses *J. Therm. Stresses* **19** 237–65
[8] He X Q, Ng T Y, Sivashanker S and Liew K M 2001 Active control of FGM plates with integrated piezoelectric sensors and actuators *Int. J. Solids Struct.* **38** 1641–55
[9] Kawai T, Miyazaki S and Araragi M 1990 A new method for forming a piezoelectric FGM using a dual dispenser system *Proc. 1st Int. Symp. on Functionally Gradient Materials (Sendai, Oct. 1990)* ed M Yamanouchi, M Koizumi, T Hirai and I Shiota, pp 191–6
[10] Ichinose N, Miyamoto N and Takahashi S 2004 Ultrasonic transducers with functionally graded piezoelectric ceramics *J. Eur. Ceram. Soc.* **24** 1681–5
[11] Cao X, Jin F and Jeon I 2009 Rayleigh surface wave in a piezoelectric wafer with subsurface damage *Appl. Phys. Lett.* **95** 261906
[12] Collet B, Destrade M and Maugin G A 2006 Bleustein–Gulyaev waves in some functionally graded materials *Eur. J. Mech.* A **25** 695–706
[13] Du J, Jin X, Wang J and Xian K 2007 Love wave propagation in functionally graded piezoelectric material layer *Ultrasonics* **46** 13–22
[14] Liu N, Yang J, Qian Z and Hirose S 2010 Interface waves in functionally graded piezoelectric materials *Int. J. Eng. Sci.* **48** 151–9
[15] Kwon S M 2003 On the dynamic propagation of an anti-plane shear crack in a functionally graded piezoelectric strip *Acta Mech.* **167** 73–89
[16] Chen J and Liu Z 2005 On the dynamic behavior of a functionally graded piezoelectric strip with periodic cracks vertical to the boundary *Int. J. Solids Struct.* **42** 3133–46
[17] Liu G R and Tani J 1994 Surface waves in functionally gradient piezoelectric plates *J. Vib. Acoust.* **116** 440–8
[18] Salah I B, Njeh A and Ghozlen M H B 2012 A theoretical study of the propagation of Rayleigh waves in a functionally graded piezoelectric material (FGPM) *Ultrasonics* **52** 306–14
[19] Liu J and Wang Z 2005 The propagation behavior of Love waves in a functionally graded layered piezoelectric structure *Smart Mater. Struct.* **14** 137–46
[20] Jin F, Qian Z, Wang Z and Kishimoto K 2005 Propagation behavior of Love waves in a piezoelectric layered structure with inhomogeneous initial stress *Smart Mater. Struct.* **14** 515–23
[21] Achenbach J and Balogun O 2010 Anti-plane surface waves on a half-space with depth-dependent properties *Wave Motion* **47** 59–65
[22] Kim Y and Hunt W 1990 Acoustic fields and velocities for surface acoustic wave propagation in multilayered structures: an extension of the Legendre polynomial approach *J. Appl. Phys.* **68** 4993–7
[23] Lefebvre J, Zhang V, Gazalet J, Gryba T and Sadaune V 2001 Acoustic wave propagation in continuous functionally graded plates: an extension of the Legendre polynomial approach *IEEE Trans. Ultrason. Ferroelectr. Freq. Control* **48** 1332–40
[24] Yamada K, Sakamura J and Nakamura K 2001 Equivalent network representation for thickness vibration modes in piezoelectric plates with a linearly graded parameter *IEEE Trans. Ultrason. Ferroelectr. Freq. Control* **48** 613–6

[25] Gao L, Wang J, Zhong Z and Du J 2009 An analysis of surface acoustic wave propagation in functionally graded plates with homotopy analysis method *Acta Mech.* **208** 249–58
[26] Chen J, Pan E and Chen H 2007 Wave propagation in magneto-electro-elastic multilayered plates *Int. J. Solids Struct.* **44** 1073–85
[27] Salah I B, Wali Y and Ghozlen M H B 2011 Love waves in functionally graded piezoelectric materials by stiffness matrix method *Ultrasonics* **51** 310–6
[28] Chen W, Lee K Y and Ding H 2005 On free vibration of non-homogeneous transversely isotropic magneto-electro-elastic plates *J. Sound Vib.* **279** 237–51
[29] Cao X, Jin F and Kishimoto K 2012 Transverse shear surface wave in a functionally graded material infinite half space *Phil. Mag. Lett.* **92** 245–53
[30] Yang J, Jin Z and Li J 2008 On the shear stress distribution between a functionally graded piezoelectric actuator and an elastic substrate and the reduction of its concentration *IEEE Trans. Ultrason. Ferroelectr. Freq. Control* **55** 2360–2
[31] Joshi S P 1992 Non-linear constitutive relations for piezoceramic materials *Smart Mater. Struct.* **1** 80–3
[32] Bouhdima M S, Zagrouba M and Ghozlen M H B 2012 The power series technique and detection of zerogroup velocity Lamb waves in a functionally graded material plate *Can. J. Phys.* **90** 159–64
[33] Abdalla A N, Alsheikh F and AlHossain A Y 2009 Effect of initial stresses on dispersion relation of transverse waves in a piezoelectric layered cylinder *Mater. Sci. Eng.* B **162** 147–54
[34] Jiang S, Jiang Q, Li X, Guo S, Zhou H and Yang J 2006 Piezoelectromagnetic waves in a ceramic plate between two ceramic half-spaces *Int. J. Solids Struct.* **43** 5799–810
[35] Liu J, Wang Y and Wang B 2010 Propagation of shear horizontal surface waves in a layered piezoelectric half-space with an imperfect interface *IEEE Trans. Ultrason. Ferroelectr. Freq. Control* **57** 1875–9
[36] Mindlin R D 1967 Bechmann's number for harmonic overtones of thickness/twist vibrations of rotated Y-cut quartz plates *J. Acoust. Soc. Am.* **41** 969–73
[37] He H, Liu J and Yang J 2011 Thickness-shear and thickness-twist vibrations of an AT-cut quartz mesa resonator *IEEE Trans. Ultrason. Ferroelectr. Freq. Control* **58** 2050–5
[38] Cao X, Jin F, Jeon I and Lu T 2009 Propagation of Love waves in a functionally graded piezoelectric material (FGPM) layered composite system *Int. J. Solids Struct.* **46** 4123–32